

Quantitative Nuclear Evaporation Theory. II. Proton Evaporation*

DAVID B. BEARD†

University of California, Davis, California

AND

ALDEN MCLELLAN‡

University of California, Davis, California

(Received 20 May 1965)

The transmission of protons into an infinitely absorbing Eckart-Bethe diffuse-nuclear-potential well has been calculated exactly as a function of nuclear size, proton energy, and angular momentum. The transmission varies by an order of magnitude from that computed by others in the critical energy range where the peak of the evaporated proton spectrum occurs. The computed transmission is used to calculate the spectra of protons emitted from excited nuclei and the reaction cross sections for (p,pn) , $(p,2n)$, and $(p,2p)$ processes. The fit with experimental data is excellent.

I. INTRODUCTION

IN a previous paper¹ treating neutron evaporation we derived a quantitative theory of nuclear level densities in a diffuse nuclear potential using no parameters based on evaporation experiments. This work was a modification and extension of Bethe's² basic theory. The theory of the evaporation of particles from an excited nucleus proceeds from a consideration of detailed balance³; hence, the result includes the cross section for the inverse process, the capture cross section of the particle by an already excited nucleus. In contrast to the ease with which neutron capture cross sections may be approximated, the Coulomb barrier greatly complicates the calculation of proton capture cross sections. A few of the publications which have contributed a great deal to our present understanding of charged-particle reactions are the ones by Bethe and Konopinski,⁴ Bethe,² Blatt and Weisskopf,³ Huizenga and Igo,⁵ Scott,⁶ and Kikuchi.⁷

Theoretical proton transmissions are very sensitive to the assumed nuclear-well shape, positive-charge distribution, and calculational approximations used in their derivation. The use of a square well,³ point positive charge, or the WKB approximation⁷ may affect the spectral shape and cause the total reaction cross section to vary by more than an order of magnitude from an exact calculation using a more realistic potential and charge distribution. The optical-model well has also been used with parameters fitted by scattering experiments from nuclei in their ground state. Unfortunately, the capture cross sections of nuclei, while in a highly

excited state, are what are needed and the use of the imaginary part of the optical-model ground-state nuclear potential violates the fundamental assumption of the evaporation theory that the mean free path of a nucleon in the nucleus is much shorter than the nuclear radius. It is more consistent with this fundamental assumption to assume that the nucleus will absorb all protons which penetrate into the nuclear well and reduce the computation of inverse proton cross sections to a computation of the transmission through the Coulomb barrier.

A numerical solution to the radial wave function for a proton in a diffuse Eckart-Bethe (Woods-Saxon) nuclear potential and a Hofstadter charge distribution is presented in Sec. II as a function of nuclear size and proton energy and angular momentum. The calculation of neutron spectra presented previously¹ has been extended and refined to include proton evaporation in Sec. III. A calculation of proton spectra and multiple-particle-reaction cross sections for which experimental data exists is given in Sec. IV; the agreement is well within the uncertainties introduced by an uncertain knowledge of competition with gamma emission and neglect of nuclear shell effects occurring at low excitation energy. The results are summarized in Sec. V where a discussion is given of the relevance of this calculation to our long-range effort of analyzing high excitation (~ 100 MeV) in terms of the properties of nuclear matter.

II. PROTON TRANSMISSION THROUGH THE COULOMB BARRIER

We assume an incident proton experiences a potential field of force given by an attractive diffuse nuclear potential given by (i)

$$V_{\text{nucl}} = -V_0[1 + \exp\eta(r-R)]^{-1}, \quad (1)$$

where the constants, V_0 , R , and η have been fitted from low-energy scattering experiments⁸ to be $V_0=42$ MeV, $R=1.35 A^{1/3}$ F, and $\eta=1.45$ F⁻¹, and (ii) a repulsive

⁸ A. A. Ross, H. Mark, and R. D. Lawson, Phys. Rev. **102**, 1613 (1956).

* Assisted by the U. S. Atomic Energy Commission, Contract No. AT(11-1)-34 Project 26.

† Now at the University of Kansas, Lawrence, Kansas.

‡ Now at the University of Nevada, Reno, Nevada.

¹ D. B. Beard and A. McLellan, Phys. Rev. **131**, 2664 (1963).

² H. A. Bethe, Rev. Mod. Phys. **9**, 69 (1937).

³ J. Blatt and V. F. Weisskopf, *Theoretical Nuclear Physics* (John Wiley & Sons, Inc., New York, 1952).

⁴ E. V. Konopinski and H. A. Bethe, Phys. Rev. **54**, 130 (1938).

⁵ J. R. Huizenga and G. I. Igo, Nucl. Phys. **29**, 462 (1962).

⁶ J. M. C. Scott, Phil. Mag. **45**, 441 (1954).

⁷ Ken Kikuchi, Progr. Theoret. Phys. (Kyoto) **17**, 643 (1957).

electrostatic potential given by

$$\begin{aligned}
 V_{\text{Hof}} &= -\frac{Z}{r_2} + \frac{\pi\rho_0}{3} \left(\frac{r_2^3 - 2r_2r_1^2 + r_1^3}{r_2 - r_1} - \frac{r_1^3}{r_2} \right) + \frac{2\pi\rho_0}{3} (r_1^2 - r^2); & r < r_1 \\
 &= -\frac{Z}{r_2} + \frac{\pi\rho_0}{3(r_2 - r_1)} \left[(r_2^3 - 2r_2r^2 + r^3) - \frac{(r_2 - r)r_1^4}{rr_2} \right]; & r_1 < r < r_2 \\
 &= Z/r, & r_2 < r,
 \end{aligned} \tag{2}$$

where

$$\rho_0 = (3/\pi)Z/(r_1 + r_2)(r_1^2 + r_2^2).$$

Z is the atomic number of the target nucleus and r_1 and r_2 are given by Hahn, Ravenhall, and Hofstadter⁹ to be

$$r_1 = 1.07 A^{1/3} - 1.5 \text{ F}, \quad \text{and} \quad r_2 = 1.07 A^{1/3} + 1.5 \text{ F}.$$

Thus the Schrödinger equation for the radial wave function of the proton $R_l = U_l/r$ is

$$\frac{d^2U_l}{dr^2} + \frac{2M}{\hbar^2} \left[V_{\text{nuel}} + V_{\text{Hof}} + \frac{\hbar^2}{2M} l(l+1) \right] U_l = 0. \tag{3}$$

The effective potentials for two representative wave functions are illustrated in Figs. 1 and 2. It is convenient to represent the effective potential by the convenient approximate potential suggested by Kikuchi⁷:

$$\begin{aligned}
 V &= -V_1 + V_2 e^{-b(a-r)}, & r < a \\
 &= 2V_2 - V_1 - V_2 e^{-b(r-a)}, & a < r < c \\
 &= Z/r + (\hbar^2/2M)l(l+1)/r^2, & c < r,
 \end{aligned} \tag{4}$$

where the constants V_1 , V_2 , a , b , and c are chosen to best fit the actual effective potential. The approximate potential is also illustrated in Figs. 1 and 2.

The solutions for $r < c$ are Bessel functions of complex argument and order.

$$U_l = J_n[2i((2MV_2)^{1/2}/\hbar b) \exp -b(a-r)/2], \quad r < a \tag{5}$$

$$U_l = J_{ip}[2(\sqrt{2MV_2}/\hbar b) \exp -b(r-a)/2], \quad r > a, \tag{6}$$

where

$$n = 2[2m(E + V_1)]^{1/2}/\hbar b$$

and

$$p = 2[2m(E - 2V_2 + V_1)]^{1/2}/\hbar b.$$

For $r > c$ the solutions are the well-known Coulomb wave functions.¹⁰ These solutions are matched by means of an IBM-1620 computer and the transmission of each partial wave is thus obtained in an elementary way (see, for example, Beard¹¹). The partial-wave transmissions

$T_l(E)$ for three representative nuclei are illustrated in Figs. 3-5. The partial cross sections, $\pi\lambda^2(2l+1)T_l(E)$, are shown for three representative nuclei in Figs. 6-8.

The total cross section is also very useful to have

$$\sigma_{\text{tot}}(E) = \sum_l \pi\lambda^2(2l+1)T_l(E).$$

The total cross section is graphed in Fig. 9 for Yb¹⁷⁰ and compared to the geometrical cross section, two experimental points, and an early exact calculation given by Blatt and Weisskopf³ for a square well with radius $1.5A^{1/3}$ F. It is apparent that even the use of as large a nuclear radius as $1.5A^{1/3}$ F (instead of the more realistic radius of $1.35A^{1/3}$ F) causes the transmission to be significantly underestimated in the critical proton energy range of 5-10 MeV where most of the proton emission occurs. The increase in transmission that occurs from using a diffuse nuclear well rather than a square well has been stressed some time ago by Kikuchi⁷

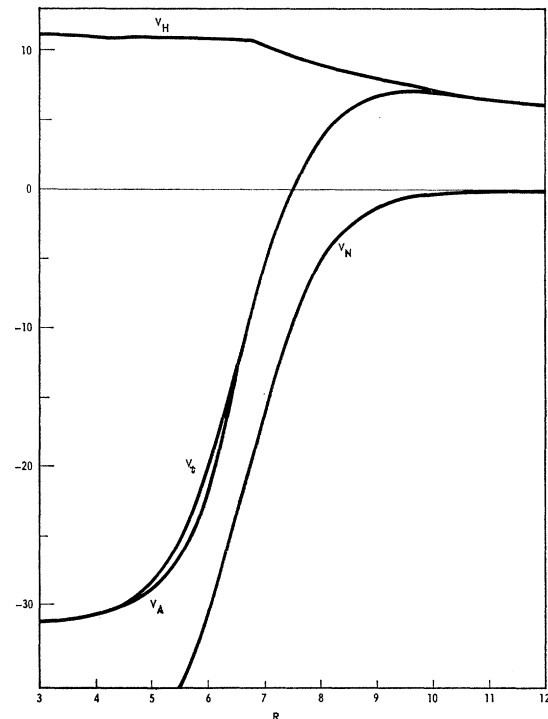


FIG. 1. Nuclear V_N , electrostatic V_H , total V_T , and approximate V_A , radial potentials for Sn with $l=0$, $r_0=1.35$; R is in fermi, V in MeV.

⁹ B. Hahn, D. G. Ravenhall, and R. Hofstadter, Phys. Rev. **101**, 1131 (1956).

¹⁰ Milton Abramowitz, *Tables of Coulomb Wave Functions* (U. S. Department of Commerce, National Bureau of Standards, Applied Mathematics Series No. 17, Washington, D. C., 1952).

¹¹ D. B. Beard, *Quantum Mechanics* (Allyn and Bacon, Inc., Boston, Massachusetts, 1963).

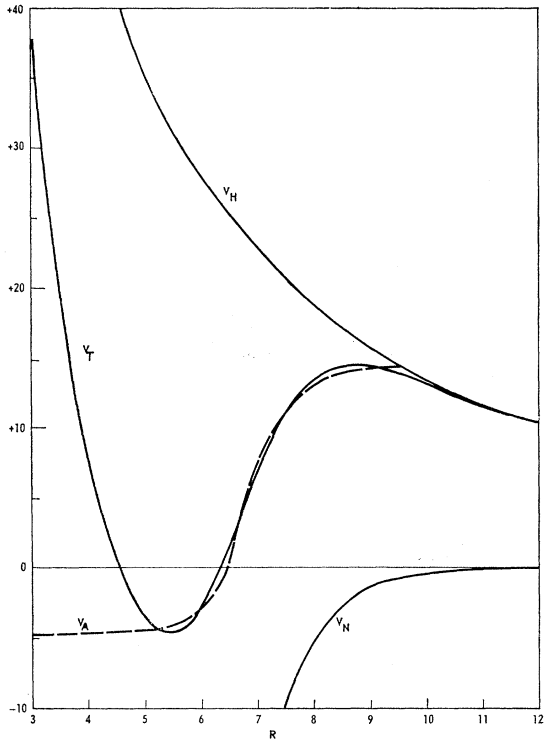


FIG. 2. Nuclear V_N , electrostatic plus angular momentum V_H , total V_T , and approximate V_A radial potentials for Sn with $l=5$. $r_0=1.35$; R is in fermi, V in MeV.

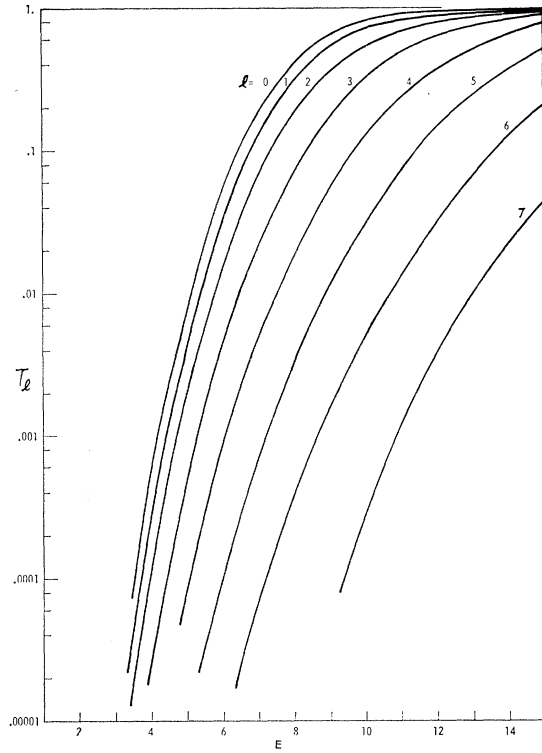


FIG. 4. Transmissions T_l as a function of E in MeV for Nd for $l=0-7$.

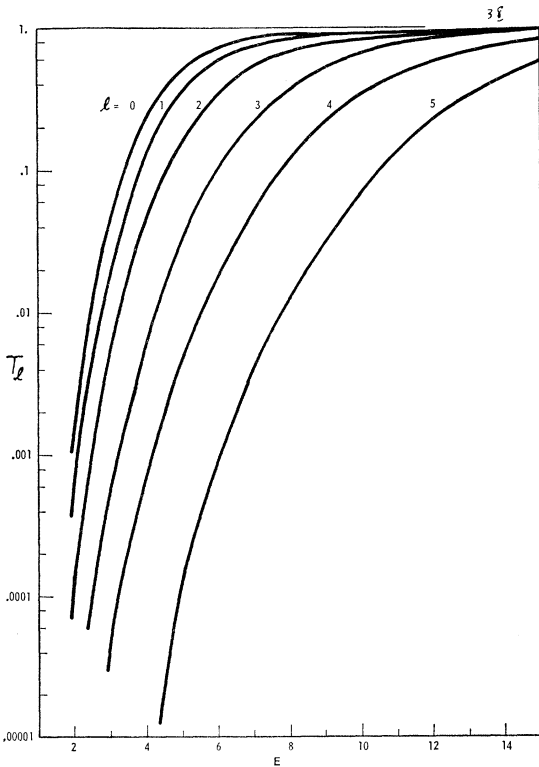


FIG. 3. Transmissions T_l as a function of E in MeV for Zn for $l=0-5$.

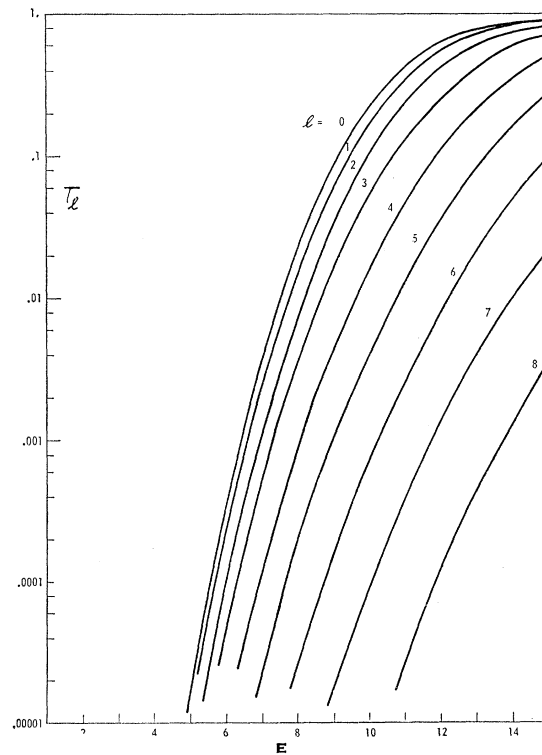


FIG. 5. Transmissions T_l as a function of E in MeV for Th for $l=0-8$.

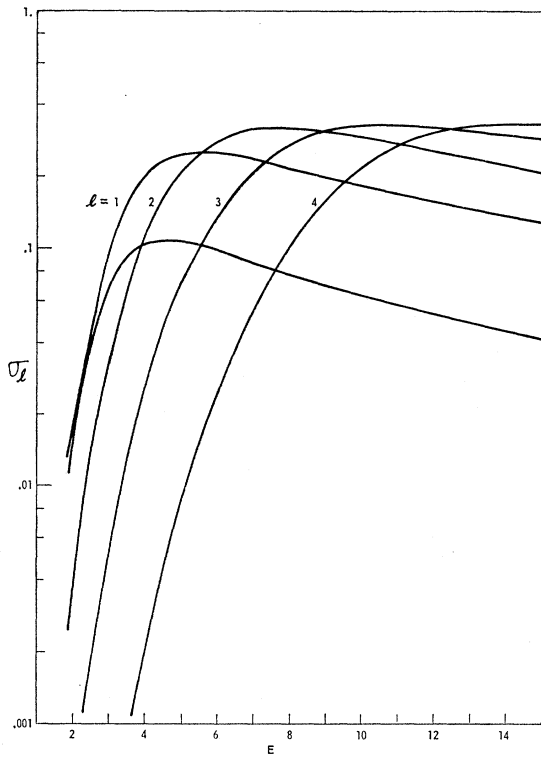


FIG. 6. Partial cross section σ_l in barns as a function of E in MeV for Ca for $l=0-4$. Nuclear potential radius $1.35 A^{1/3}$ F.

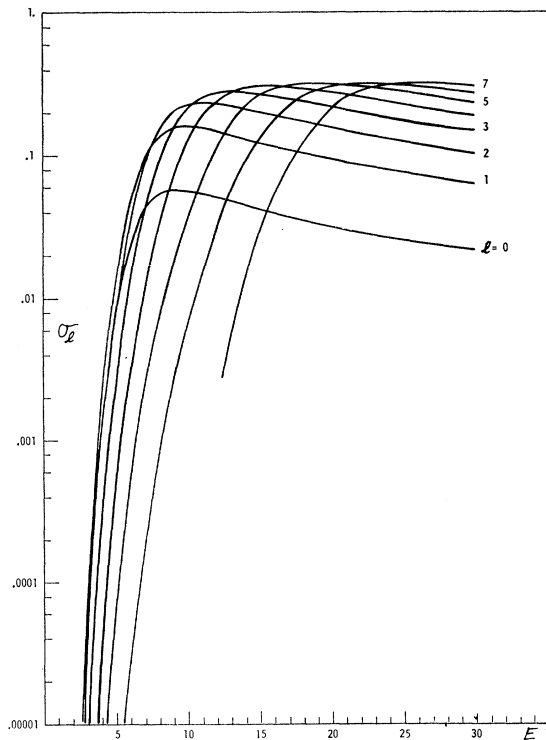


FIG. 7. Partial cross section σ_l in barns as a function of E in MeV for Sn for $l=0-7$. Nuclear potential radius $1.35 A^{1/3}$ F.

who used the WKB approximation to illustrate his point. We have found that the WKB approximation differs significantly from the more exact calculation but it does suggest a convenient exponential form as given below in Eq. (8), which represents our numerically obtained results.

The total cross sections for nuclei whose atomic numbers differ by ten are graphed in Fig. 10. A satisfactory fit to these curves is obtained with a simple formula

$$\sigma_{\text{total}}(E) = \pi R^2 [1 + (1 + 10/z)(\alpha/E)^{1.5}] \times \exp[-(\alpha/E)^{1.5}], \quad (8)$$

where Z is the target nucleus atomic number, A is the target atomic mass number, R is the target radius $1.35 A^{1/3}$ F, and $\alpha = 1.50 + 0.289Z$.

The effect of varying the radius of the nuclear potential, as might occur due to thermal expansion for a highly excited nucleus, is illustrated in Fig. 11 for the total cross section of Sn for various nuclear potential radii. The electrostatic potential was unchanged. Blatt and Weisskopf's total cross section for a square nuclear potential with two different radii are also shown for comparison.

A similar calculation of the neutron cross section was also undertaken and the results are satisfactorily represented by

$$\sigma_{\text{total}}^n(E) = \pi(R + \lambda)^2 [1 - \exp(-BE^N)], \quad (9)$$

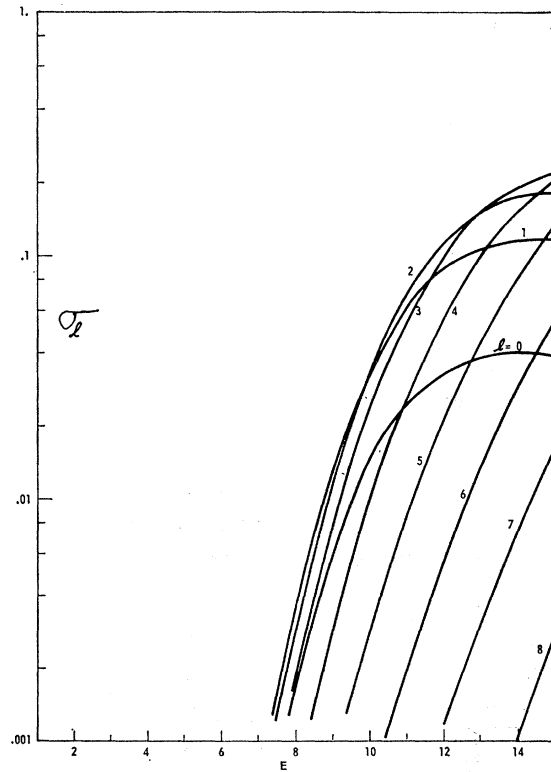


FIG. 8. Partial cross section σ_l in barns as a function of E in MeV for Th for $l=0-8$. Nuclear potential radius $1.35 A^{1/3}$ F.

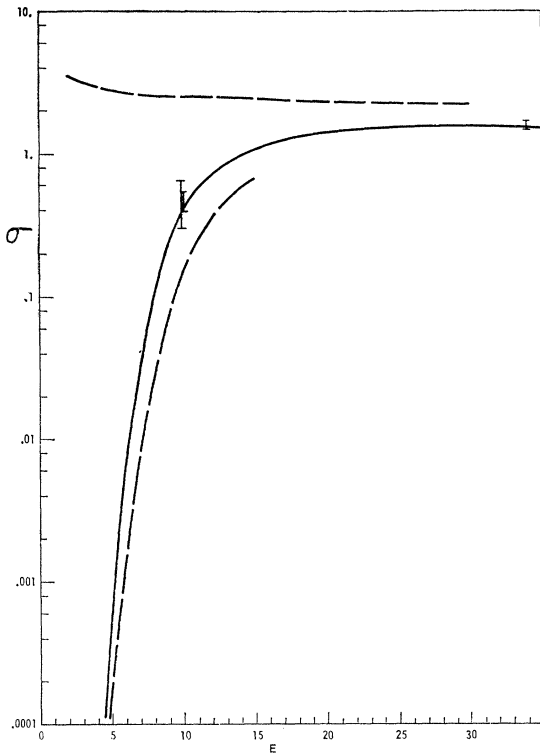


FIG. 9. Total cross section σ_t in barns as a function of E in MeV for Yb. Upper dashed curve is geometrical cross section, $\pi(R+\lambda)^2$, in the absence of electrostatic repulsion. The solid curve is our calculated cross section for a nuclear potential "radius" of $1.35A^{1/3}$ fermi. This result was extrapolated beyond 15 MeV so as to match the experimental results at energies higher than 15 MeV where the nucleus should appear completely absorptive. Experimental points are shown at $E=10$ and 34 MeV. Lower dashed curve is Blatt and Weisskopf's calculation for a square nuclear potential with radius $1.5A^{1/3}$ fermi.

where

$$B = 2.144 - 0.0813A^{1/3} \quad \text{and} \quad N = 0.7834 - 0.0414A^{1/3}.$$

This result differs from that found by Feld *et al.*¹² and used in our earlier work.¹ However, the customary approximation to the neutron capture cross section πR^2 was found to be adequate for the calculations reported below.

III. PROTON EVAPORATION

The emission of a particle with energy between E and $E+dE$ from a nucleus with energy E_m and angular-momentum quantum number J has been derived by Erickson,¹³ Vandenbosch and Huizenga,¹⁴ Thomas,¹⁵

¹² B. T. Feld, H. Feshbach, M. L. Goldberger, H. Goldstein, and V. F. Weisskopf, Final Report of the Fast Neutron Data Project NYO-636, Atomic Energy Commission Document, 1951 (unpublished).

¹³ T. Erickson, Nucl. Phys. **11**, 481 (1959).

¹⁴ R. Vandenbosch and J. R. Huizenga, Phys. Rev. **120**, 1313 (1960).

¹⁵ T. D. Thomas, Nucl. Phys. **53**, 558 (1964).

and others and may be expressed as

$$N(E, J)dE = KE\omega_0(E_m - B - E) \sum_{j=0}^{\infty} (2j+1) \\ \times \exp[-\hbar^2(j+\frac{1}{2})^2\alpha_0^{1/2}/2C(E_m - B - E)^{1/2}] \\ \times \sum_{s=|j-s|}^{j+s} \sum_{l=|J-s|}^{J+s} \sigma_c(l, E)dE, \quad (10)$$

where K is a normalization factor which is a function of J and E_m , $\omega_0(E_m - B - E)$ is the total level (or rather state) density of the residual nucleus summed over all angular momenta,¹ j is the angular-momentum quantum number of the residual nucleus, α_0 is the level density parameter,¹ c is the rigid-body moment of inertia, s and l are the spin and orbital-momentum quantum numbers of the emitted particle $\mathbf{S} = \mathbf{s} + \mathbf{j}$, and $\sigma_c(l, E)$ is the capture cross section of the residual nucleus with excitation energy $E_m - B - E$ for a particle with energy E , binding energy B , and orbital-momentum quantum number l .

$\sigma_c(l, E)$ is negligible for $l > (2ME)^{1/2}r_0A^{1/3}/\hbar$ where $(2ME)^{1/2}$ is the linear momentum of the emitted particle, and $r_0A^{1/3}$ is the radius of the residual nucleus. Therefore a compound nucleus with large angular-momentum quantum number J may have its emission of low-energy particles limited by the factor

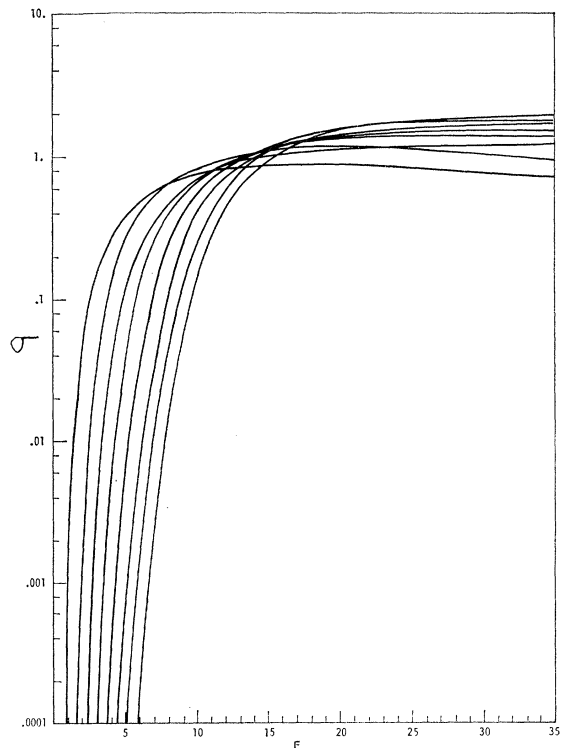


FIG. 10. Calculated total cross sections σ_t in barns, as a function of energy for $Z=20, 30, 40, 50, 60, 70, 80,$ and 90 . Cross section for $Z=20$ is at left. Higher Z curves proceed monotonically to right.

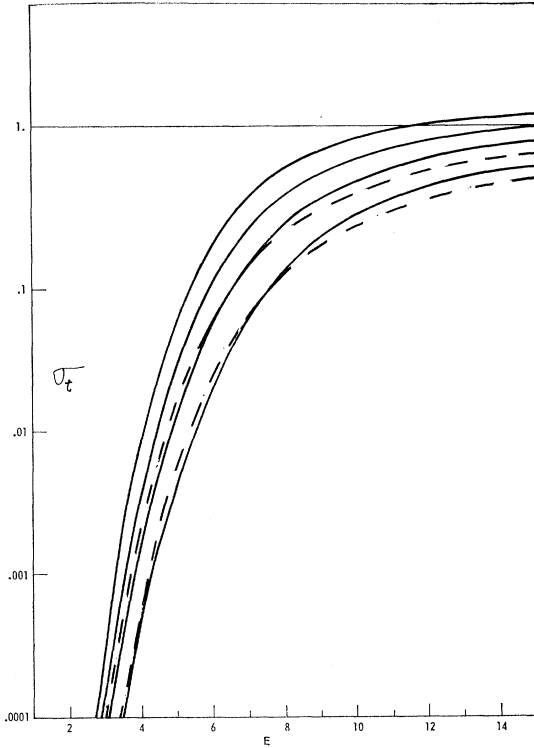


FIG. 11. Calculated total cross section of Sn in barns for nuclear potential "radii" of $r_0 A^{1/3}$ with solid curve at left for $r_0 = 1.5$ F. Next three solid curves are for $r_0 = 1.35, 1.2,$ and 1.0 F, respectively. Dashed curves represent Blatt and Weisskopf's results for a square nuclear potential of $r_0 = 1.5$ F at left and $r_0 = 1.3$ F at right. Horizontal line at 1.4 barns is for $\sigma_t = \pi R^2 = \pi (1.35 A^{1/3})^2$.

$\exp[-(j + \frac{1}{2})^2 (\alpha_0)^{1/2} 2c(E_m - B - E)^{1/2}]$. In general, the summations indicated in Eq. (10) must be undertaken with the help of the curves illustrated in Figs. 6-8. Other curves may be obtained by writing to one of us. Several approximations have been given for large J (see, for example, Knox *et al.*¹⁶ and Thomas^{15,17}), but these approximations are useful mainly when the compound nucleus was formed by absorption of an energetic multiple charged ion. For inelastic neutron scattering at 14 MeV we have found that the neutron spectra were unaffected if the effects of angular momentum were neglected. Thomas^{15,17} has examined this question with considerable care and has found that for rigid-body moments of inertia the effects of angular momentum may be represented by small changes in the power of the excitation energy in the coefficient of the exponential term occurring in the expression for $\omega_0(E_m - B - E)$.

Since the evaporation spectra are a very insensitive function of this coefficient and since Thomas' result was obtained for 20-MeV alpha particles on V^{51} , we will neglect the angular-momentum effects throughout our analysis of compound nuclei which have much less

angular momenta. We are thus enabled to use Eq. (8) for the total inverse proton cross section [Eq. (7)] and Eq. (10) then becomes

$$N_{1p}(E)dE = KE\omega_0(E_m - B - E)\pi R^2 \times [1 + (1 + 10/Z)(\alpha/E)^{1.5}] \exp[-(\alpha/E)^{1.5}]dE, \quad (11)$$

where the level density in the residual nucleus, $\omega_0(E_m - B - E)$, has been derived by many authors and has been given by us¹ approximately as

$$\omega_0(E_m - B - E) = (1/2\pi)\alpha_0^{1/4}(E_m - B - E)^{-3/4} \times \exp\{2[\alpha_0(E_m - B - E)]^{1/2}\}, \quad (12)$$

where α_0 is a parameter derived entirely independently of evaporation experiments and is equal to $0.0933A$, A being the atomic mass number of the residual nucleus.

The normalization constant K is determined by requiring that the total probability that the excited nucleus decays by proton, neutron, or gamma emission must be one.

$$K = \left\{ \int_0^{E_m - B_p} N_{1p}(E)dE + \int_0^{E_m - B_n} N_{1n}(E)dE + \Gamma_{\text{tot}}(\gamma) \right\}^{-1}. \quad (13)$$

The relative probability of emitting a gamma ray may be roughly estimated from comparing an estimate of the lifetime of a 1-MeV gamma ray for decay to a particular residual level, 10^{-11} sec, to the number of times a 1-MeV neutron strikes the "walls" of the nucleus, $R/v \sim 10^{-12}/10^9 = 10^{-21}$ sec. Hence, when a 1-MeV neutron may be emitted $\Gamma_{\text{tot}}(\gamma)$ is negligible even though the excitation energy of the residual nucleus may be 8 MeV higher after a 1-MeV gamma ray is emitted than after a 1-MeV neutron is emitted. The probability of proton emission includes the factor $\sigma_{e^p}(E)$ and when neutrons cannot be emitted, $\Gamma_{\text{tot}}(\gamma)$ is an appreciable factor in considering the evaporation of low-energy protons. Evaporation of protons to residual nuclei of low excitation energy ($\sim 1-2$ MeV) is further complicated by the necessity to include shell structure effects¹⁸⁻²⁰ in the residual level density expression in a precise calculation.

Multiple-particle emission is calculated by integrating over the spectrum of earlier emitted particles. For example, the spectrum of the second emitted proton in a two-proton decay process is

$$N_{2p}(E)dE = \int_0^{E_m - B_{1p} - B_{2p} - E} EK_2(E') \times \omega_0(E_m - B_{1p} - B_{2p} - E - E') \sigma_{e^p}(E) E' K_1 \omega_0 \times (E_m - B_{1p} - E') \sigma_{e^p}(E') dE' dE, \quad (14)$$

¹⁶ W. J. Knox, A. R. Quinton, and C. E. Anderson, *Phys. Rev.* **120**, 2120 (1960).

¹⁷ T. D. Thomas, *Nucl. Phys.* **53**, 577 (1964).

¹⁸ C. Bloch, *Phys. Rev.* **93**, 1094 (1954).

¹⁹ N. Rosenzweig, *Phys. Rev.* **105**, 950 (1957); **108**, 817 (1957).

²⁰ A. A. Ross, *Phys. Rev.* **108**, 720 (1957).

where $K_2(E')$ is given by

$$K_2(E') = \left\{ \int_0^{E_m - B_{1p} - B_{2p} - E'} N_{2p}(E, E') dE + \int_0^{E_m - B_{1p} - B_{2n} - E'} N_{2n}(E, E') dE + \Gamma_{\text{tot}}(\gamma) \right\}^{-1}, \quad (15)$$

$N_{2p}(E, E')$ and $N_{2n}(E, E')$ being the spectra of second emitted particles (proton or neutron) with energy E following a first proton with energy E' . When the first emitted particle is a neutron, σ_c^p in (14) must be replaced by $\sigma_c^n \sim \pi R^2$. Fortunately, when the first emitted particle is a neutron most of the residual nuclei are left

in a higher state of excitation than for proton initial emission and have approximately the same excitation since the neutron spectrum peaks sharply at neutron energies around one or two MeV. Hence an adequate and simple approximation to (15) may frequently be made by setting E' equal to a constant (say zero) and avoiding the complicated twofold integration implicit in Eqs. (14) and (15). This approximation was made in our previous work¹ and can be made here for $(x, n\bar{p})$ reactions, but the full labor of the twofold integration must be undertaken for $(x, 2\bar{p})$ reactions.

It is frequently convenient and adequate to use the method of steepest descent or the temperature approximation to the residual level density in performing the integrations in Eq. (15). Thus

$$\int_0^{E \gg E_0'} N_p(E') dE' \sim K \sigma_c^p(E_0') [\alpha_0(-f'')]^{-1/2} \exp[4\alpha_0(E_m - B_p)]^{1/2} T^{-3/2} \exp(-E_0'/T), \quad (16)$$

where

$$\begin{aligned} T &= [(E_m - B_p)/\alpha_0]^{1/2}, \\ E_0' &\sim (1.5T)^{0.4} \alpha_0^{0.6} [1 - 0.17(T/\alpha_0)^{0.6}], \\ f'' &\sim -2.04/T^{1.4} \alpha_0^{0.6}; \\ \int_0^{E \gtrsim E_0'} N_p(E') dE' &= \int_0^\infty N_p(E') dE' - K(ET + T^2) \exp(-E/T) \sigma_c^p(E) (2\pi\alpha_0)^{1/2} T^{-3/2} \exp[4\alpha_0(E_m - B_p)]^{1/2}; \quad (17) \\ \int_0^{E > T} N_n(E') dE' &= K \sigma_c^n (T/2\pi\alpha_0)^{1/2} \exp[4\alpha_0(E_m - B_n)]^{1/2} \{1 - (1 + E/T) \exp(-E/T)\}, \quad (18) \end{aligned}$$

where $E_m - B_n$ is the maximum possible residual excitation energy and $T = [(E_m - B_n)/\sigma\alpha_0]^{1/2}$.

The spectrum of protons emitted following neutron emission is given approximately by

$$N(E) dE \sim \text{const} \sigma_c^p(E) Q_2^{-3/4} \times \exp(2\alpha_0 Q_2)^{1/2} (1/T_1 + 1/T_2)^{-2} dE, \quad (19)$$

where

$$T_1 = [(E_m - B_n)/\alpha_0]^{1/2}, \quad Q_2 = E_m - B_n - B_p - E,$$

and

$$T_2 = (Q_2/\alpha_0)^{1/2}.$$

IV. COMPARISON WITH A FEW REPRESENTATIVE EXPERIMENTS

Allan²¹ has measured the proton spectra emitted in the backward direction resulting from 14-MeV (d, t) neutron bombardment of Fe^{54} . The binding energies of the possible emitted particles are such that only first emitted protons and protons following neutron emission need to be considered since the $(n, 2\bar{p})$ reaction is negligible compared with the $(n, \bar{p}n)$ reaction. Binding energies of the possible reaction products were obtained from Baker's²² mass formula and substituted into Eqs.

(11) and (19) and the result is compared to the experimental observation in Fig. 12. The excellent fit much below 3 MeV is entirely fortuitous in view of the uncertainty in binding energies, gamma-ray competition, the theoretical approximations to the level density (ignoring shell effects at low energy), the integrals in Eq. (15), and the use of Eq. (19) at low excitation energy.

The absolute number of protons emitted as second emitted particles is adjusted to form a best fit to the experimental points although it was not necessary to normalize the $(n, n'\bar{p})$ proton distribution in this way. Fifteen percent of the first emitted particles are protons. Twenty-six percent of the first emitted neutrons leave the Fe^{54} nucleus sufficiently excited to emit a proton with energy greater than 3.5 MeV below which energy the uncertain knowledge of level density and gamma-ray competition obviates the necessity for a precise calculation. The $(n, 2n)$ and $(n, 2\bar{p})$ processes are negligible because of the 14-MeV binding energy of a neutron in Fe^{54} and the competition of the $(n, \bar{p}n)$ process after the first proton in Fe^{55} is evaporated. Therefore, the area under the curves for the (n, \bar{p}) process and the $(n, n'\bar{p})$ process should be approximately equal (15% \sim 0.85 \times 26%) as indeed they are for the two curves in Fig. (12).

²¹ D. L. Allan, Nucl. Phys. **10**, 348 (1959).

²² G. A. Baker Jr., Can. J. Phys. **34**, 423 (1956).

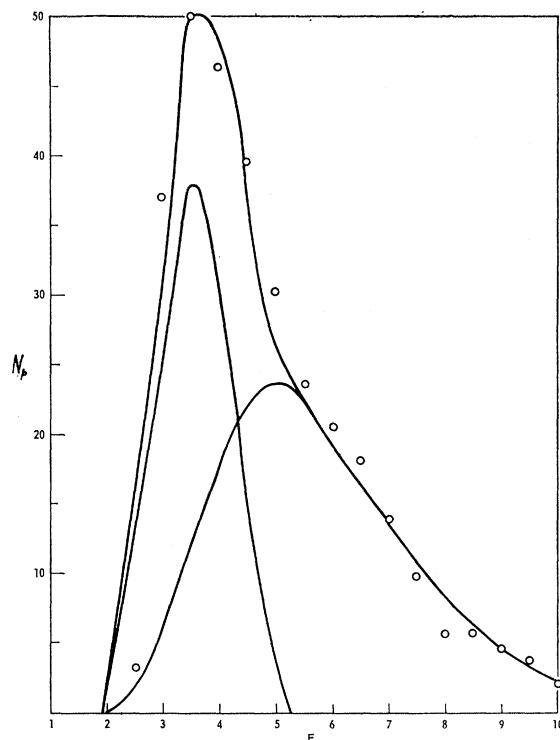


FIG. 12. Proton spectra from Fe^{54} bombarded by 14-MeV neutrons. Experimental points (Ref. 21) are indicated by \circ . Lower curve at right is the calculated (n,p) process; lower curve at left is the calculated $(n,n'p)$ process with the magnitude adjusted so that the upper curve, representing the total proton spectra, best fits the experimental data.

Paul and Clarke²³ have observed the total (n,p) reaction cross section for 14-MeV neutron bombardment of many nuclei by observing the radioactivity induced in the target. The results for our analysis, based on Baker's²² binding energies of a few representative nuclei which are uncomplicated by possible unobserved competing processes, are given in Table I and compared with experimental and Paul and Clarke's theoretical estimates. Our theoretical estimates of proton emission are lower than those of Paul and Clarke, but this is in the right direction since evaporation of protons is relatively improbable and the total cross section for proton reactions includes direct interactions which are equally probable.

Cohen and Rubin²⁴ have measured proton spectra

TABLE I. Calculated and observed cross sections (in millibarns) for proton production by 14-MeV neutrons.

Target atom	P	Ti	V	Ni	Se
Observed $\sigma(n,p)$	64	93	27	182	45
Calculated, Paul and Clarke $\sigma(n,p)$	205	325	164	196	168
Calculated, this work $\sigma(n,p)$	51	36	8.7	75	28

²³ E. B. Paul and R. L. Clarke, Can. J. Phys. 31, 267 (1953).

²⁴ B. L. Cohen and A. G. Rubin, Phys. Rev. 113, 579 (1959).

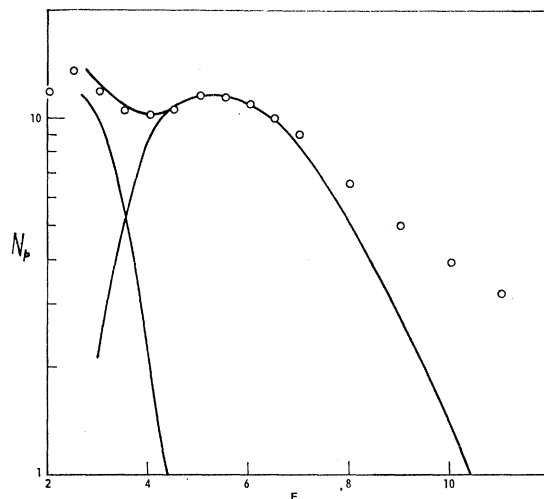


FIG. 13. Proton spectra from Cu bombarded by 14.9-MeV protons. Experimental points (Ref. 24) are indicated by \circ . Calculated curves are for (p,p') at right, $(p,2p) + (p,np)$ at left, and the sum of the two curves.

evaporated from a copper target after bombardment by protons of various energies. Binding energies of possible reaction products were obtained from Baker's²² mass formula and substituted into Eqs. (11), (14), and (19) and the result is compared to their measurements for incident proton energies of 14.9 and 23 MeV in Figs. 13 and 14. The poor fit at the high-energy portion of the spectrum is to be expected since these protons are primarily products of the direct-interaction process and not due to compound-nucleus decay. The heights of the second emitted particle curves were fitted to the experimental results. The spectrum below 2 MeV is subject to

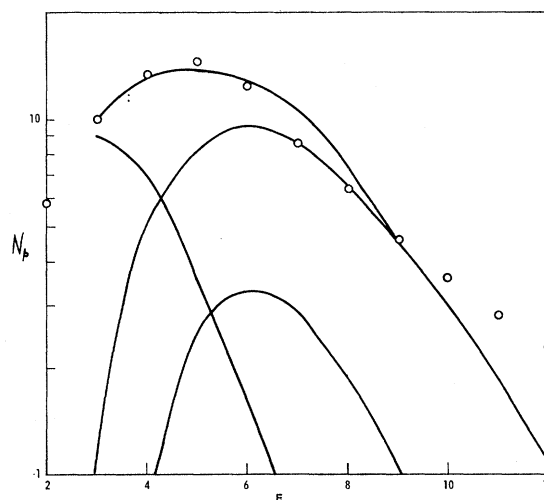


FIG. 14. Proton spectra from Cu bombarded by 23-MeV protons. Experimental points (Ref. 24) are indicated by \circ . Calculated curves are the (p,p') process at right, the (p,np) process at lower center, the $(p,2p)$ process at left, and the total of the calculated proton spectra.

the ever-prevalent uncertainties in this work due to the use of our higher energy approximation to the level density in the residual nucleus and the rough estimate of the competition due to gamma rays.

Cohen, Newman, and Handley²⁵ have measured the total cross sections for $\sigma(p,2p)$ and $\sigma(p,np)+\sigma(p,2n)$ for 21.5-MeV protons incident on Ni⁶⁸ and Zn⁶⁸. These are especially useful measurements to compare with theory since relatively few of the direct-interaction processes leave the nucleus with sufficient energy to emit a second particle. Our binding energies were obtained from Wing and Varley's²⁶ tables. Our computed results are compared with the experimental measurements in Table II. Considering the uncertainty in binding energy upon which the cross sections are very sensitively dependent, the agreement is gratifyingly good despite the large differences in cross sections for Zn⁶⁸.

V. CONCLUSIONS

The partial cross sections for the absorption of a proton by an excited nucleus have been computed by matching wave functions at the edge of an Eckart-Bethe (Woods-Saxon) diffuse nuclear potential including an electrostatic repulsion based on a Hofstadter nuclear positive charge distribution. The partial cross sections for nuclei of atomic number 20, 30, 40, 60, 70, 80, and 90 are presented in Figs. 6-8 and the total cross sections are presented in Fig. 10 and in the approximate formula, Eq. (8). As can be readily seen from Figs. 10-14, the electrostatic barrier transmission dominates the proton emission in the energy region where the majority of the protons are emitted. Proton spectra are thus more dependent on an accurate calculation of the inverse cross section than on the expression used for the level density in the residual nucleus. The spectra and, in particular, the various reaction cross sections are extremely sensitive to the size and shape of the nuclear and electrostatic potentials. Earlier estimates of the inverse cross section differ by an order of magnitude from our results as indicated by two of the pioneering estimates illustrated in Figs. 9 and 11.

Expressions for proton spectra resulting from (x,p) , (x,np) , and $(x,2p)$ processes are given in Eqs. (11), (14), and (19) and some spectra are illustrated in Figs. 12-14. These spectra fit the experimental data shown in these figures very well. Because of the sensitive dependence of the total proton emission on the electrostatic barrier transmission an even better test of the theory is the estimate of the total reaction cross sections given in Tables I and II. Table I of the (n,p) cross section also lists Paul and Clarke's experimental observations which give significantly higher cross sections than

we have calculated. Since a significant part of their experimental cross sections are due to protons produced by direct interactions, their experiment does not contradict the theory, but it does not support it very well either; their experiment merely suggests the relative importance of direct interaction and compound processes. Table II, listing the theoretical and experimental cross sections for multiple particle emission is, however, crucially significant. It is unlikely that the direct interaction process contributes significantly to multiple particle emission, particularly the $(x,2p)$ process, because the nucleus resulting from direct interaction is left in too low an excitation to emit a second particle, particularly a proton.

TABLE II. Calculated and observed $\sigma(p,np)+\sigma(p,2n)$ and $\sigma(p,2p)$, in mb.

	$\sigma(p,np)+\sigma(p,2n)$		$\sigma(p,2p)$	
	Calculated	Experimental	Calculated	Experimental
Ni ⁶⁸	260	240	580	680
Zn ⁶⁸	950	>780	7.2	3.8

In all of our comparison of our theoretical estimates with experiment we believe that the greatest uncertainty lies in our knowledge of the binding energies of the various emitted particles on which the spectra and reaction cross sections depend very sensitively. The low-energy portion of the proton spectra (below ~ 3 MeV) is also quite uncertain because of the crudeness of our approximation of the competition from gamma-ray emission and our neglect of the shell-structure effects near the ground states of the residual nuclei. A more exact treatment of the latter may be obtained from the excellent work of Bloch,¹⁸ Rosenzweig,¹⁹ Ross,²⁰ and others. For very high excitation energies, particularly when the excitation is induced by heavy multiply charged ions, angular-momentum effects become important and cannot be neglected as we have done in the experimental comparison presented in Sec. IV. In this instance other approximations must be used in Eq. (10) than the one we have adopted, and/or the partial cross sections illustrated in Figs. 6-8 must be used.

As discussed in greater detail in our previous paper,¹ our primary objective is to be able to analyze particle spectra from nuclei excited to ~ 100 MeV in the hope of detecting significant experimental departures from the present theory which could be interpreted reliably in terms of a change in the size and shape of the nuclear potential. This in turn would lead to an estimate of the compressibility and other properties of nuclear matter. First, however, we wished to be sure of thoroughly understanding the spectra from nuclei excited to 10-30 MeV in terms of our knowledge of nuclei in their ground state. This we have done in our previous paper for neutron spectra in which the neutron spectra were calculated entirely without the use of parameters

²⁵ B. L. Cohen, E. Newman, and T. H. Handley, Phys. Rev. **99**, 723 (1955).

²⁶ J. Wing and J. D. Varley, Argonne National Laboratory Report No. 6886, 1964 (unpublished).

adjusted to fit experimental evaporation data. The present calculation extends this work to proton evaporation and has given us confidence in the fundamental theory for the evaporation of any nucleon from excited nuclei whose charge and nuclear force distribution are known from other kinds of measurements on nuclei in their ground state. With respect to our long range objective, a very satisfying feature of the proton emission is the enhanced sensitivity of the pro-

ton emission on the potential shape over that of the level density on the potential shape.

The authors are very grateful to Professor Donald A. Norton and the Davis Computer Center in general for the seemingly infinite time made available on the IBM-1620 computer required for computing the electrostatic barrier transmission. The authors are also indebted to Professor Wm. W. True for his interest and support of this work.

PHYSICAL REVIEW

VOLUME 140, NUMBER 4B

22 NOVEMBER 1965

Nuclear Size Determination by Neutral-Pion Photoproduction

ROALD A. SCHRACK

National Bureau of Standards, Washington, D. C.

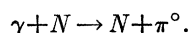
(Received 18 March 1965)

The angular distributions of neutral pions produced by 166-MeV bremsstrahlung on Li, Be, C, O, Mg, Al, Si, S, Ca, and Cu have been obtained by coincident detection of the pion decay photons. The density distributions of nuclear matter have been inferred from the experimental data by means of a Monte Carlo synthesis based on an impulse-approximation elastic-coherent-production model.

INTRODUCTION

THIS paper presents the results of a recently completed set of experiments and their analysis. In a previous paper by Schrack, Leiss, and Penner (SLP) the technique of pion photoproduction as a means of nuclear size determination was investigated using the complex nuclei C, Al, Cu, Cd, and Pb.¹ The results presented in that paper were in general agreement with the results obtained by electron scattering. This set of measurements was initiated to improve and extend the technique and to try to resolve some of the questions that arose as a result of the first series of measurements.

The general layout and experimental method used in this experiment is essentially the same as that used in SLP. A bremsstrahlung beam of peak energy 166 MeV, obtained from the NBS electron synchrotron, was used to photoproduce neutral pions from a variety of complex nuclei (N):



The decay photons from the neutral pions were detected in coincidence in a set of counters designed to provide good determination of the colatitude angle of the pions. Modifications of the equipment from the SLP setup were:

(1) The counter system was altered to improve the shape of the angular sensitivity of the counters to the incident photons. This was done to allow better analytic

representation of the counter in the Monte Carlo synthesis used to analyze the data.

(2) The x-ray beam and target were placed in a vacuum pipe to reduce backgrounds.

(3) Mechanical stability of the system was improved to permit more precise target and counter placement.

(4) Shielding and collimation were improved.

In addition, the analysis was refined to include the effects of the electron pulse shape of the synchrotron, x-ray beam alignment, target size, and counter angular-sensitivity shape. A more complete description of the experimental and analytical technique is given elsewhere.^{1,2}

THEORY

The angular distribution of neutral pions obtained by photoproduction from complex nuclei has been explained on the basis of an elastic coherent model in which the spin-independent part of the interaction plays the only important role.¹⁻³ Under these assumptions the cross section in the center-of-mass system for production of pions of momentum k at angle θ is

$$\sigma(k, \theta) = A^2 F^2(q) (\sin^2 \theta) \sigma_p(k),$$

where A is the mass number of the nucleus, $\sigma_p(k)$ is the spin-independent pion photoproduction cross section from hydrogen, and $F(q)$ is the elastic form factor of the

¹ R. A. Schrack, J. E. Leiss, and S. Penner, *Phys. Rev.* **127**, 1772 (1962).

² R. A. Schrack, Ph.D. thesis, University of Maryland, 1960 (unpublished).

³ J. E. Leiss and R. A. Schrack, *Rev. Mod. Phys.* **30**, 456 (1958).